Electronic Supplementary Material (ESI) for Faraday Discussions.
This journal is © The Royal Society of Chemistry 2023

Supplementary Information

Morphology, dynamic disorder, and charge transport in an indoloindole-based hole-transporting material from a multi-level theoretical approach

Manuel Pérez-Escribano,[a,†] Alberto Fernández-Alarcón,[a,†] Enrique Ortí,[a] Juan Aragó,[a] Jesús Cerdá,[b,*] Joaquín Calbo[a,*]

[a] Instituto de Ciencia Molecular, Universidad de Valencia, 46890 Paterna, Spain
[b] Laboratory for Chemistry of Novel Materials, Materials Research Institute, University of Mons-UMONS, Mons 7000, Belgium

E-mail: jesus.cerdacalatayud@umons.ac.be; joaquin.calbo@uv.es

[†] These authors contributed equally

Kinetic Monte Carlo

The electronic mobility has been evaluated using the kinetic Monte Carlo approach[1] implemented in a home-made code. In the kinetic Monte Carlo, we perform a stochastic dynamic simulation of the hopping of a single charge carrier. We use the direct method based on Gillespie algorithm,[2,3] where an adaptative timestep (τ) is calculated as:

$$\tau = -\frac{\ln(r_1)}{a_0} \tag{1}$$

where r_1 is a random number and a_0 is the summation of the rate constants corresponding to all possible charge hopping paths, $a_0 = \sum_i k_i$. On the other hand, the direction of each individual hop is decided by using a second random number (r_2) according to the following condition:

$$\frac{\sum_{1}^{i-1} k_i}{a_0} < r_2 < \frac{\sum_{1}^{i} k_i}{a_0} \tag{2}$$

where at each hop, the rate constants are computed according to the classical Marcus rate expression.[4] Additionally, in order to take into account the instantaneous fluctuations due to the dynamical disorder, *V* and Δ*E* are obtained for each hop according to:

$$V = \text{gauss\_random}(r_3, \langle V \rangle, \sigma_V) \tag{3}$$

$$\Delta E = \text{gauss\_random}(r_4, \langle \Delta E \rangle, \sigma_{\Delta E}) + q\mathbf{Fr} \tag{4}$$

where gauss_random is a function that computes a random number (r_3 and r_4) according to a normal distribution with given parameters (mean value and standard deviation) previously obtained, *q* is the charge, **r** is the displacement vector for the hopping path, and **F** is the applied electric field along the measured direction.

The position of the charge carrier is tracked along the hopping dynamics and the final charge mobility (μ) is computed with a similar expression to those used in master equation approaches:[5,6]

$$\mu = \frac{\mathbf{rF}}{t|F|^2} \tag{5}$$

where **r** is the total displacement vector from the initial to the last charge carrier position at the end of the kinetic simulation, *t* is the time at the end of the simulation and F is the applied electric field.

Table S1. Crystal cell parameters for IDIDF.

Structure	a (Å)	b (Å)	c (Å)	α (°)	β (°)	γ (°)
Experimental	5.535	13.714	17.791	68.19	82.84	80.89
DFT	5.549	13.943	17.746	67.13	81.42	79.53
DFT+vdW	5.011	13.077	18.790	66.51	80.73	81.95

Table S2. Crystal cell parameters for spiro-OMeTAD.

Structure	a (Å)	b (Å)	c (Å)	α (°)	β (°)	γ (°)
Experimental	13.661	14.720	17.277	86.23	68.98	80.01
DFT	13.782	14.629	17.554	85.72	69.37	79.52
DFT+vdW	13.316	14.531	17.015	86.26	68.42	79.88

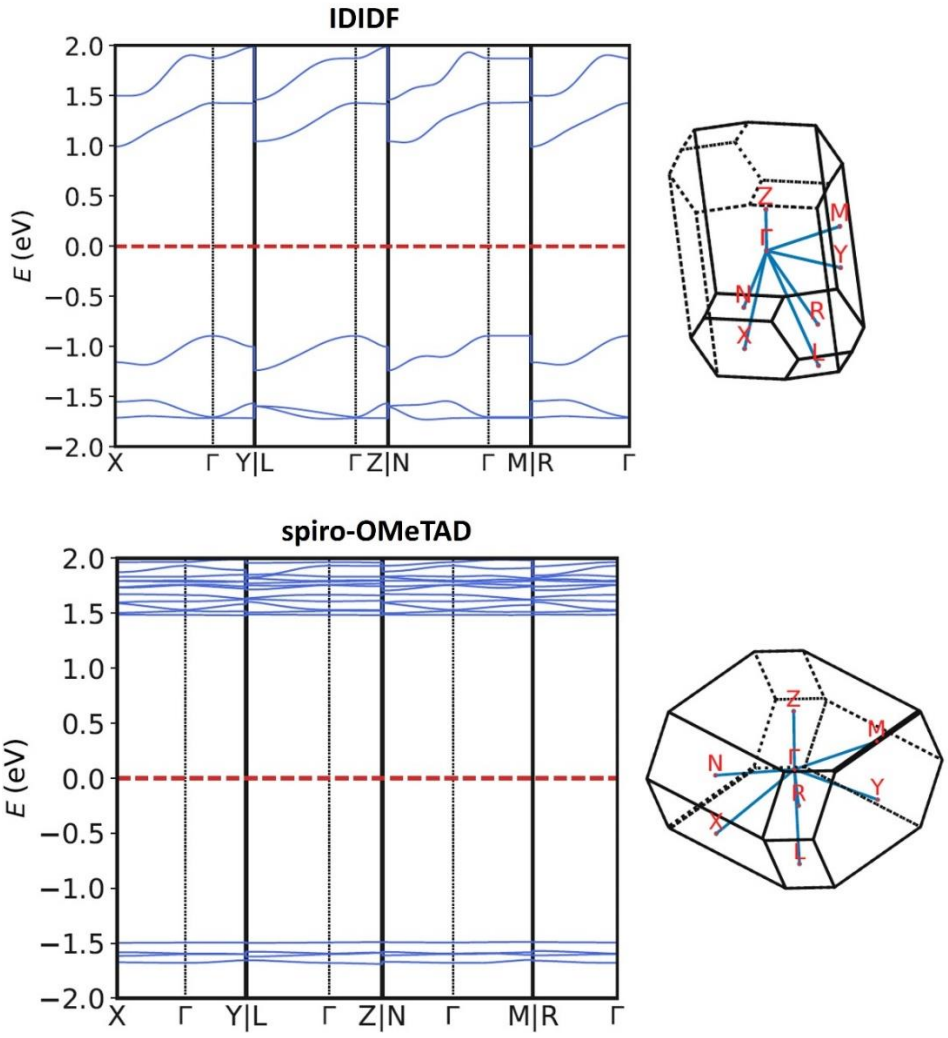

Figure S1. Band structure diagrams for spiro-OMeTAD (left) and IDIDF (right) calculated at the HSE06 level along the full k-path of the Brillouin zone $X-\Gamma-Y|L-\Gamma-Z|N-\Gamma-M|R-\Gamma$ according to the centrosymmetric triclinic space group $P\bar{1}$ of spiro-OMeTAD and IDIDF.

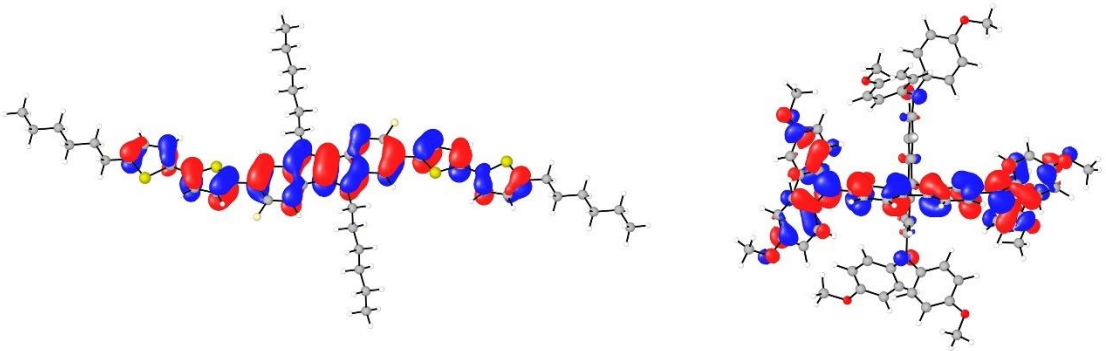

Figure S2. Highest-occupied molecular orbitals calculated at the XXX level for IDIDF (left) and spiro-OMeTAD (right).

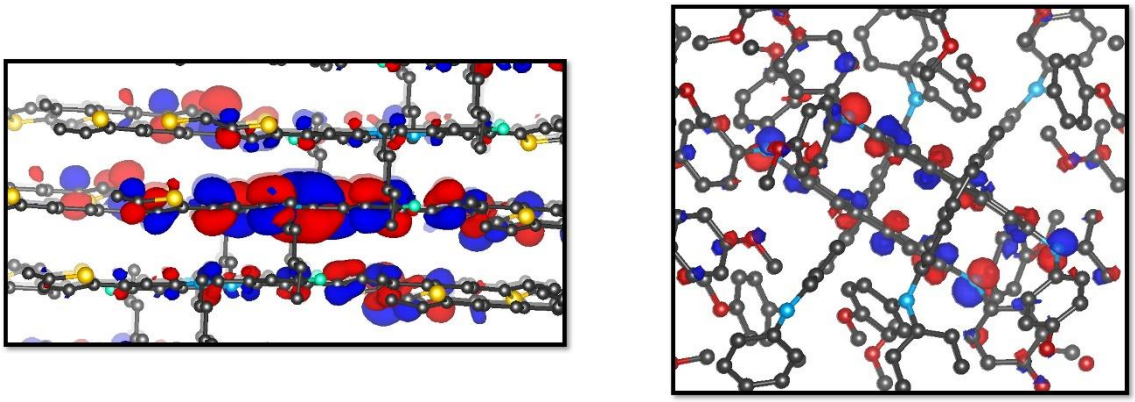

Figure S3. Crystal orbital representations of the valence band maximum (VBM) calculated at the HSE06 level of theory on the PBEsol-optimized geomtries for IDIDF (left) and spiro-OMeTAD (right).

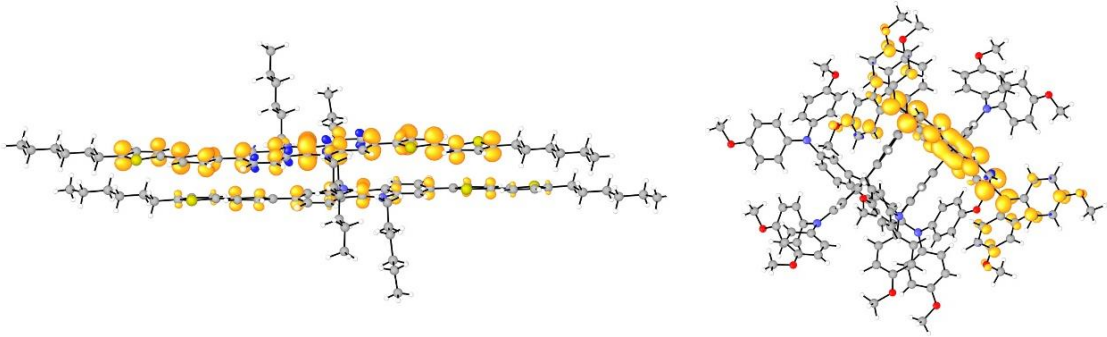

Figure S4. Spin density (isovalue = 0.01) calculated for the most interacting dimers of IDIDF (left) and spiro-OMeTAD (right) where one neutral molecule is replaced by its minimum-energy geometry in the cation state.

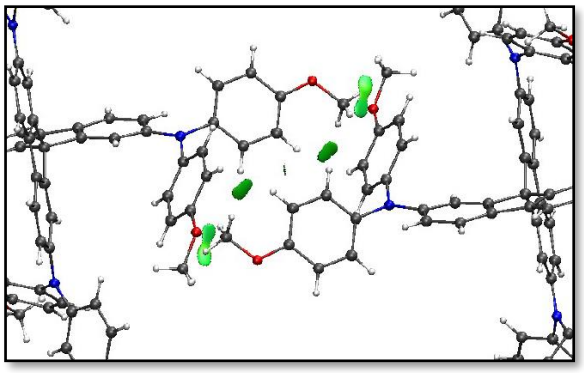

Figure S5. Non-covalent surfaces calculated for the $1\bar{1}\bar{1}$ dimer of spiro-OMeTAD, which possesses an electronic coupling of 2 meV.

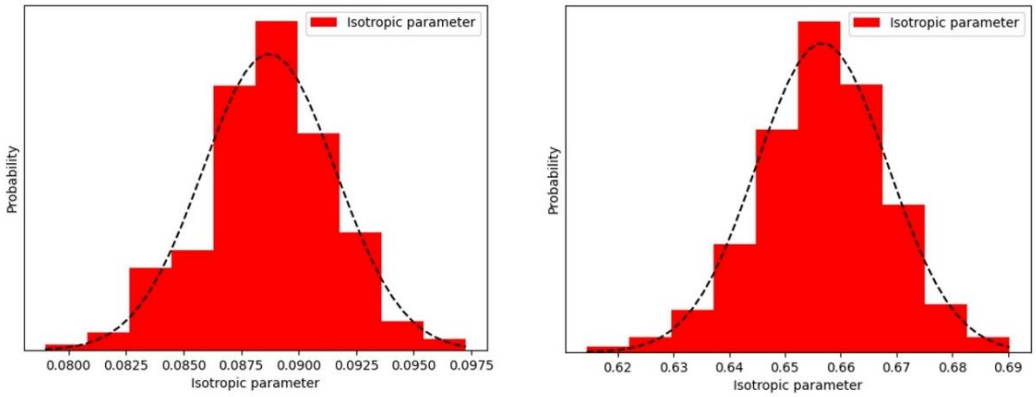

Figure S6. Normal distribution of the isotropic ISO parameter calculated for one molecule of IDIDF (left) and spiro-OMeTAD (right) HTMs along the molecular dynamics of the crystalline phase. The distribution parameters are: $\bar{X}$ = 0.0887, σ = 0.003; and $\bar{X}$ = 0.6567, σ = 0.012 for IDIDF and spiro-OMeTAD, respectively.

Table S3. Maximum values for the hole mobility calculated in each crystallographic axis and the mean value obtained considering all the crystallographic planes explored (*ab*, *bc*, and *ac*) in the static crystals (0 K) and considering dynamic disorder (298 K) for IDIDF and spiro-OMeTAD.

	$\mu_{a\text{-axis}}$	$\mu_{b\text{-axis}}$	$\mu_{c\text{-axis}}$	μ_{mean}
IDIDF				
Crystal (0 K)	6.806	0.509	2.938	3.361
Crystal (298 K)	2.285	0.161	0.901	1.078
spiro-OMeTAD				
Crystal (0 K)	0.301	0.115	0.093	0.150
Crystal (298 K)	0.041	0.002	0.004	0.014

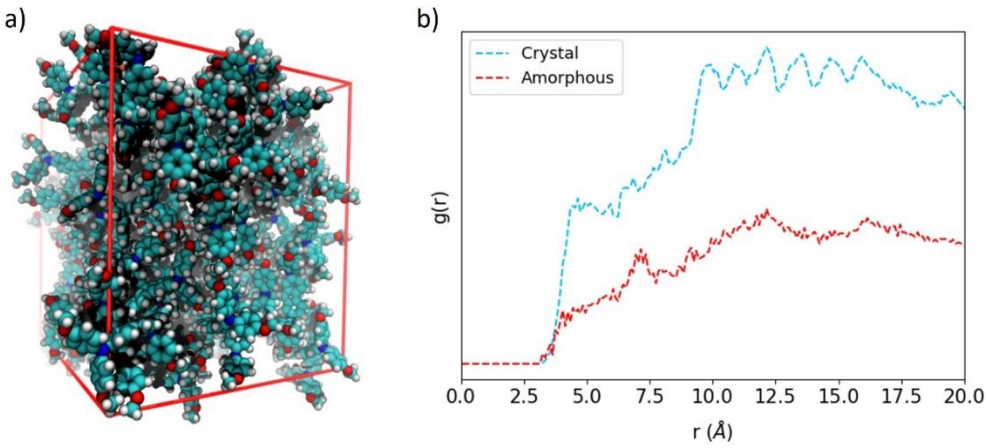

Figure S7. a) Representative snapshot of the amourphous spiro-OMeTAD phase. b) Radial distribution function of the centroid of a central molecule with respect to the other molecules in crystalline and amorphous spiro-OMeTAD.

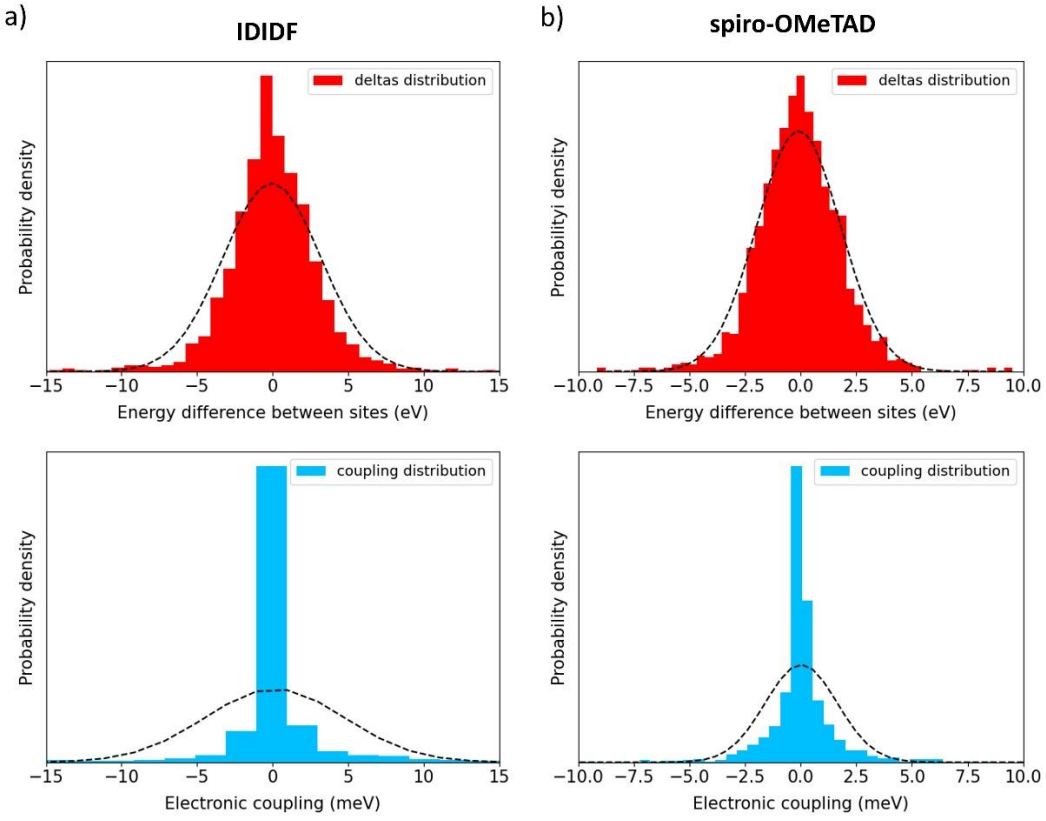

Figure S8. Normal distributions for the site energy (top) and dimer electronic coupling (bottom) of IDIDF (a) and spiro-OMeTAD (b) obtained along the molecular dynamics simulations of the amorphous materials.

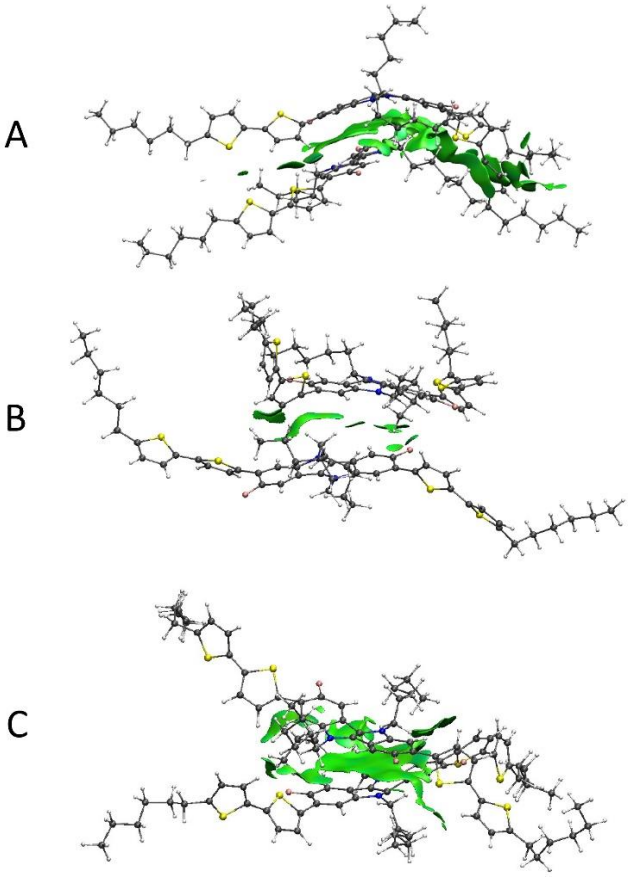

Figure S9. Non-covalent NCI surface plots of the reduced density gradient calculated using promolecular densities for dimers A, B and C of amorphous IDIDF indicated in Figure 9 of the main text.

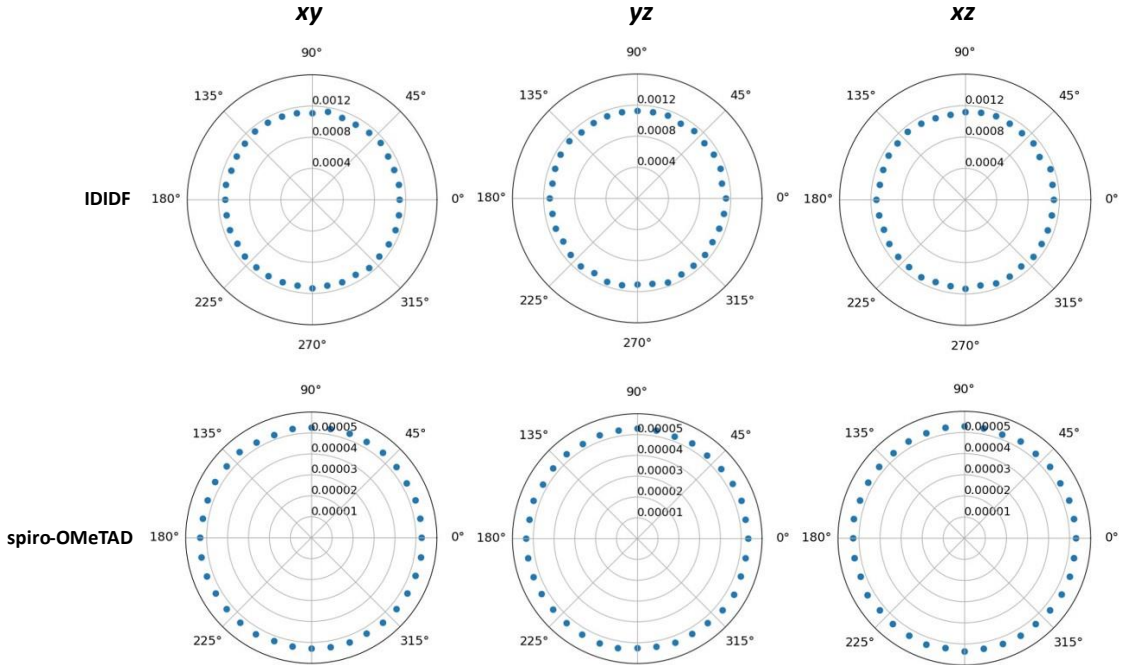

Figure S10. Hole mobilities calculated along the *xy*, *yz* and *xz* planes for the amorphous materials of IDIDF and spiro-OMeTAD.

References

1 H. Li and J. L. Brédas, *J. Phys. Chem. Lett.*, 2017, **8**, 2507–2512.

2 D. R. D'hooge, A. D. Trigilio, Y. W. Marien and P. H. M. van Steenberge, *Ind. Eng. Chem. Res.*, 2020, **59**, 18357–18386.

3 D. T. Gillespie, *J. Comput. Phys.*, 1976, **22**, 403–434.

4 R. A. Marcus, *Rev. Mod. Phys.*, 1993, **65**, 599.

5 V. Stehr, R. F. Fink, M. Tafipolski, C. Deibel and B. Engels, *Wiley Interdiscip. Rev. Comput. Mol. Sci.*, 2016, **6**, 694–720.

6 V. Stehr, J. Pfister, R. F. Fink, B. Engels and C. Deibel, *Phys. Rev. B*, 2011, **83**, 155208.